UNIVERSITY OF WEST BOHEMIA

Applied and Computational Mechanics 1 (2007) 521 - 530

Applied and Computational Mechanics

Smoothed particle hydrodynamics modelling of fluids and solids

L. Lobovský[a,*], J. Křen[a]

[a] *Department of Mechanics, Faculty of Applied Sciences, UWB in Pilsen, Univerzitní 22, 306 14 Plzeň, Czech Republic*

Received 16 September 2007; received in revised form 10 October 2007

Abstract

The study is concerned about the application of the smoothed particle hydrodynamics (SPH) method within the computational fluid dynamics and elastodynamics. A brief description of the SPH model for an incompressible fluid and for an elastic solid is presented. The implemented model of incompressible fluid is tested for internal flows as well as for flows involving a free surface of the fluid. The implemented elastic solid model is examined during the simulation of the mechanical response of rubber rings.

Keywords: smoothed particle hydrodynamics, meshless methods, incompressible fluid, elastic solid

1. Introduction

The smoothed particle hydrodynamics (SPH) method is a truly meshless Lagrangian numerical technique first introduced to solve gas dynamics problems in astrophysics. The first papers on the SPH method were published by Gingold and Monaghan [2] and Lucy [5] in late 1970s. During the three decades of its existence, the SPH method spread into numerous branches of computational physics, [4]. Its meshless character makes the method very flexible and enables simulations of physical problems which might be difficult to capture by conventional grid-based methods. This contribution is concerned about its application within computational continuum mechanics with a focus on the problems of hydrodynamics and elasticity. The meshless character of the SPH method is advantageous e.g. during simulations of elastic materials undergoing large deformations, during simulations of free surface flows and fluid-structure interaction. These advantages may be well employed within industrial as well as biomedical applications.

Naturally, the reliability and the stability of the SPH simulations (as well as the stability of other numerical methods) can be endangered by unphysical numerical fluctuations under certain circumstances. That can be prevented by additional numerical stabilising terms (such as artificial viscosity, artifical stress etc.). The SPH material models (the incompressible fluid model and the elastic solid model) involving the stabilising terms are implemented and applied to several test problems. The original SPH governing equations were derived for problems, where the boundaries were in infinity or could be neglected. An application of appropriate boundary conditions is also discussed.

2. SPH model

Within the SPH formulation, the computational domain is discretised by a finite set of interpolating points (particles) with invariant coordinates in the material frame. The SPH particles

*Corresponding author. Tel.: +420 377 632 336, e-mail: lobo@kme.zcu.cz.

represent a finite mass of the discretised continuum and carry the information about all physical variables which are evaluated at their positions. The function values and their derivatives at a specific particle are interpolated from the function values at surrounding particles using the interpolating (smoothing) function and its derivatives, respectively,

$$f_i = \sum_j \frac{m_j}{\rho_j} f_j W(|\mathbf{r}_i - \mathbf{r}_j|, h), \tag{1}$$

$$\nabla_i f_i = \sum_j \frac{m_j}{\rho_j} f_j \nabla_i W(|\mathbf{r}_i - \mathbf{r}_j|, h), \tag{2}$$

where m is the mass, ρ is the density and W is the interpolating (smoothing) function with a continuous derivative $\nabla_i W$. The index i, j respectively, denotes the variables at the particle i, j respectively, and ∇_i denotes a derivative according to $\mathbf{r}_i$ which is the position vector.

The smoothing function W is defined so that its value monotonously decreases as the distance between particles increases. It has a compact support domain, which radius is defined by the smoothing length h. The smoothing function is normalised and in the limit case, when the smoothing length goes to zero, the smoothing function becomes the Dirac delta function, see [4] for details. Within this study, the cubic B-spline smoothing function is applied, [6].

2.1. Incompressible fluid

The conservation laws describing the dynamics of the incompressible fluid are discretised using the relations (1) and (2) so that a symetric form of the SPH governing equations satisfying the third Newton's law is obtained. The conservation of mass is assured by the continuity equation

$$\frac{\mathrm{d}\rho_i}{\mathrm{d}t} = \sum_j m_j (\mathbf{v}_i - \mathbf{v}_j) \cdot \nabla_i W_{ij}, \tag{3}$$

where $\mathbf{v}$ is the velocity vector and $W_{ij} = W(|\mathbf{r}_i - \mathbf{r}_j|, h)$.

The conservation of momentum is described by the Navier-Stokes equation in the form

$$\frac{\mathrm{d}\mathbf{v}_i}{\mathrm{d}t} = \mathcal{P}_i + \mathcal{V}_i + \mathbf{f}_i, \tag{4}$$

where $\mathcal{P}_i$ is the pressure term, $\mathcal{V}_i$ represents the viscous forces and $\mathbf{f}_i$ is the body force. The pressure term is derived so that

$$\mathcal{P}_i = -\sum_j m_j \left(\frac{p_i}{\rho_i^2} + \frac{p_j}{\rho_j^2} \right) \nabla_i W_{ij}, \tag{5}$$

where p is the pressure. The viscous forces are modelled by a term derived by Morris et al. [10]

$$\mathcal{V}_i = \sum_j 2\mu \frac{m_j}{\rho_i \rho_j} \frac{(\mathbf{r}_i - \mathbf{r}_j) \cdot \nabla_i W_{ij}}{|\mathbf{r}_i - \mathbf{r}_j|^2 + \eta^2} (\mathbf{v}_i - \mathbf{v}_j), \tag{6}$$

which combines a standard SPH and a finite difference approximation of the first derivative. The symbol μ stands for the dynamic viscosity and $\eta^2 = 0.01h^2$ is a corrective constant avoiding a creation of singularity when particles are approaching each other.

The presented SPH model implies the quasi-incompressible representation of the incompressible fluid through the equation of state, [6],

$$p_i = {}^0p + K\left[\left(\frac{\rho_i}{{}^0\rho}\right)^{\Gamma} - 1\right], \tag{7}$$

where K is the bulk modulus

$$K = {}^0\rho\frac{{}^0c^2}{\Gamma}. \tag{8}$$

Constants ${}^0p$ and ${}^0\rho$ indicate the initial pressure and the initial density respectively. The initial sound speed value ${}^0c$ is defined so that the resulting Mach number is less than 0.1. A constant parameter Γ is usually set equal to 7.

2.2. Elastic solid

Within the SPH model of elastic solid material, the conservation of mass is represented by the continuity equation (3) as it is done within the model of incompressible fluid. The conservation of momentum for the elastic material is derived analogously to the equation of motion (4). The resulting SPH equation of motion utilising the Einstein's summation convention according to the coordinates α and β may be written as follows

$$\frac{\mathrm{d}v_i^\alpha}{\mathrm{d}t} = \sum_j m_j\left(\frac{\sigma_i^{\alpha\beta}}{\rho_i^2} + \frac{\sigma_j^{\alpha\beta}}{\rho_j^2}\right)\frac{\partial W_{ij}}{\partial x_i^\beta} + f^\alpha. \tag{9}$$

The stress tensor σ is defined so that

$$\sigma_i^{\alpha\beta} = -p_i\delta^{\alpha\beta} + S_i^{\alpha\beta}, \tag{10}$$

where p is the hydrostatic pressure, $S^{\alpha\beta}$ is the deviatoric stress and $\delta^{\alpha\beta}$ is the Kronecker delta. The rate of change of the deviatoric stress is given according to the Jaumann's formulation of the Hooke's law

$$\frac{\mathrm{d}S_i^{\alpha\beta}}{\mathrm{d}t} = 2\mu\left(\dot\epsilon_i^{\alpha\beta} - \frac{1}{3}\delta^{\alpha\beta}\dot\epsilon_i^{\gamma\gamma}\right) + S_i^{\alpha\gamma}\Omega_i^{\beta\gamma} + \Omega_i^{\alpha\gamma}S_i^{\gamma\beta}, \tag{11}$$

where μ is the shear modulus of the modelled material, $\dot\epsilon$ and Ω are the strain rate and rotation rate tensors respectively. The hydrostatic pressure p is calculated from the state equation

$$p_i = {}^0c^2(\rho_i - {}^0\rho), \tag{12}$$

while the bulk modulus of the represented material is given so that

$$K = {}^0\rho\,{}^0c^2. \tag{13}$$

3. Stabilising terms

There is a number of cases, when the SPH simulations may suffer of instability due to their meshless Lagrangian nature. High numerical oscillations may be observed during the simulations involving shocks and an unphysical particle motion caused e.g. by the tensile instability, [8], can appear during the simulations of both incompressible fluids and elastic solids.

In order to prevent the numerical instability of the SPH calculation, two additional numerical terms, the artificial viscosity and the artificial stress, can be implemented in the corresponding equation of motion. Then, the pressure term in the Navier-Stokes equation (4) becomes

$$\mathcal{P}_i = -\sum_j m_j \left(\frac{p_i}{\rho_i^2} + \frac{p_j}{\rho_j^2} + \Pi_{ij} + R_{ij}\phi_{ij}^n \right) \nabla_i W_{ij} \tag{14}$$

and the equation of motion for the elastic solid (9) is

$$\frac{\mathrm{d}v_i^\alpha}{\mathrm{d}t} = \sum_j m_j \left(\frac{\sigma_i^{\alpha\beta}}{\rho_i^2} + \frac{\sigma_j^{\alpha\beta}}{\rho_j^2} + \Pi_{ij}\delta^{\alpha\beta} + R_{ij}^{\alpha\beta}\phi_{ij}^n \right) \frac{\partial W_{ij}}{\partial x_i^\beta} + f^\alpha. \tag{15}$$

The artificial viscosity term $\Pi_{ij}\delta^{\alpha\beta}$ is applied in order to smooth the unphysical numerical oscillations, while the artificial stress term $R_{ij}^{\alpha\beta}\phi_{ij}^n$ (note that n is the exponent) reduces the tensile instability.

3.1. Artificial viscosity

The artificial viscosity can be defined as a combination of terms analogous to bulk and von Neumann-Richtmyer viscous pressures used in finite difference methods, [9],

$$\Pi_{ij} = -\zeta_1 \frac{(c_i + c_j)(h_i + h_j)}{2(\rho_i + \rho_j)} \psi_{ij} + \zeta_2 \frac{(h_i + h_j)^2}{2(\rho_i + \rho_j)} \psi_{ij}^2, \tag{16}$$

$$\psi_{ij} = \begin{cases} \frac{(\mathbf{v}_i - \mathbf{v}_j)\cdot(\mathbf{r}_i - \mathbf{r}_j)}{|\mathbf{r}_i - \mathbf{r}_j|^2 + \eta^2}, & (\mathbf{v}_i - \mathbf{v}_j)\cdot(\mathbf{r}_i - \mathbf{r}_j) < 0, \\ 0, & (\mathbf{v}_i - \mathbf{v}_j)\cdot(\mathbf{r}_i - \mathbf{r}_j) \geq 0, \end{cases} \tag{17}$$

where ζ_1 and ζ_2 are constant artificial viscosity parameters. The term Π_{ij} is positive when particles are aproaching each other and null otherwise. The first term in the equation (16) introduces the shear and the bulk viscosity and the second term helps to prevent particle interpenetration.

3.2. Artificial stress

The artificial stress term acts as a repulsive force between particles which is increased when the separation between particles decreases. That is achieved through the scaling function ϕ_{ij} which is defined as a ratio of the smoothing function values for the actual distance between the pair of particles r_{ij} and the initial particle spacing ${}^0r$,

$$\phi_{ij} = \frac{W(r_{ij})}{W({}^0r)}. \tag{18}$$

Within the incompressible fluid model, the artificial stress value R_i is taken as

$$R_i = \xi \frac{p_i}{\rho_i^2}, \tag{19}$$

when the value of the pressure p_i is negative, and null otherwise, [8]. The value of parameter ξ is set according to the value of the exponent n and the smoothing length. In the following, the value of exponent n is set equal to 4 and ξ is taken equal to 0.3.

Within the elastic solid model, the artificial stress value is considered

$$R_i^{\alpha\beta} \sim -\xi \frac{\sigma_i^{\alpha\beta}}{\rho_i^2}, \tag{20}$$

when the value of the stress $\sigma_i^{\alpha\beta}$ is positive, and null otherwise, refer to [3] for further details.

The resulting value of the artificial stress factor between two particles is assumed

$$R_{ij}^{\alpha\beta} = R_i^{\alpha\beta} + R_j^{\alpha\beta}. \tag{21}$$

3.3. Correction of particle motion

The stability of the entire calculation may be also improved by implementing the particle motion correcting term, [7], which corrects the value of particle velocity according to the averaged velocity of all neighbouring particles

$$\frac{\mathrm{d}\mathbf{r}_i}{\mathrm{d}t} = \mathbf{v}_i + \varepsilon \sum_j 2m_j \frac{\mathbf{v}_j - \mathbf{v}_i}{\rho_i + \rho_j} W_{ij}. \tag{22}$$

A constant parameter ε is from an interval $\langle 0; 1 \rangle$. This term (sometimes called the XSPH correction term) is usually applied in order to prevent an unphysical particle motion during high speed flows and during simulations of problems involving tension.

4. Implementation

An introduction of the relations (1) and (2) enables the evaluation of the function values and their spatial derivatives without a presence of a computational grid. The connectivity of grid-based methods is replaced by the search for the neighbouring particles within the compact support domain of the smoothing function. The time integration of the SPH equations is performed by an explicit numerical integration scheme (the predictor-corrector scheme is applied within this study). When rigid boundaries are involved in the simulation, either of two implemented SPH rigid boundary representations can be applied, the ghost particles or the boundary particles.

4.1. Ghost particles

The ghost particles are created by reflecting the fluid particles in the vicinity of the boundary across its interface at every timestep, [1]. The width of the reflected region is equal to the width of the smoothing function support. In order to prevent the boundary penetration by fluid and to model the no-slip boundary conditions, the ghost particle's velocity vector is opposite to the fluid particle's one.

4.2. Boundary particles

The boundary particles consist of two sets of particles, the interface and the wall particles, [11]. The position of the boundary particles does not change in time. The interface particles are placed along the boundary surface, while the wall particles fill the boundary region to the width of the smoothing function support. The density and pressure of the wall particles is evolved through the governing equations, but the density and pressure of the interface particles is not updated. When a static rigid boundary is modelled, the velocity of all the boundary particles is equal zero.

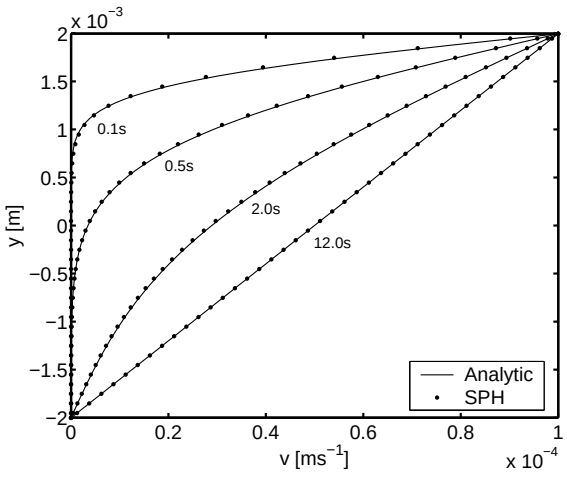

Fig. 1. Couette flow velocity profile development in time ($Re = 0.5$).

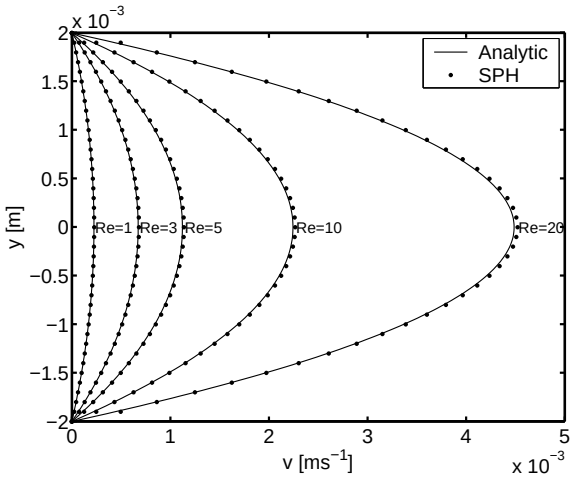

Fig. 2. Poiseuille flow resulting velocity profiles for several Reynolds numbers.

5. Numerical simulations

The performance of the implemented SPH code is examined using several examples which are given below. First, the reliability of the SPH results is tested against the analytic solution of laminar flow problems. Features of the SPH implementation of the incompressible fluid model are then employed within the periodic hill flow problem and within the free surface flow simulation. The elastic solid material model is tested on an example of a collision of two rubber rings. All simulations are performed in a two-dimensional space.

5.1. Couette and Poiseuille flow

Within both Couette and Poiseuille flow problems, the fluid is located between two parallel infinite plates. Initially, both the fluid and the walls are stationary. The Couette flow is generated by a movement of the upper plate in longitudinal direction. The plate starts to move with a constant velocity at zero time. On the contrary, the Poiseuille flow is generated by a body force acting in a longitudinal direction while both plates remain stationary. Analogously, the body force is constant and starts to act suddenly at zero time. As both Couette and Poiseuille flows can be solved analytically, the SPH solution of laminar viscous flow evolution in time can be easily examined for both studied cases, [4].

Within these simulations, the rigid boundaries are represented by the ghost particles and the periodic boundary conditions are applied in x direction. The channel width is $4\,\mathrm{mm}$, the length of the modelled channel section is $2\,\mathrm{mm}$ and the modelled fluid has the properties of water. The Couette flow velocity profile evolution in time is displayed on Fig. 1. The Reynolds number in that case is equal to 0.5. The resulting steady state solution (the solution at time when the flow becomes fully developed) of the Poiseuille flow for several values of Reynolds number is shown on Fig. 2. Both Couette and Poiseuille flow simulations are performed for relatively low Reynolds numbers. Due to the character of the rigid boundary representation, there are slight pressure waves propagating from the boundary through the fluid. As the geometry of both examples is very simple, the pressure waves are reflected and grow during the evolution of the flow. These pressure waves become significant during simulations of higher Reynolds number flows and the calculation becomes unstable. The computation can be stabilised by decreasing the sound speed value so that the artificial compressibility of the model is encreased. The

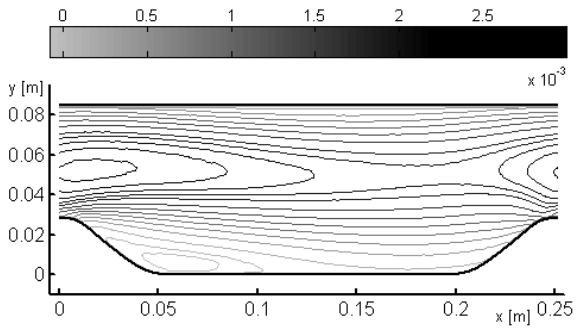

Fig. 3. Periodic hill flow: contours of velocity in x direction $[\mathrm{ms}^{-1}]$.

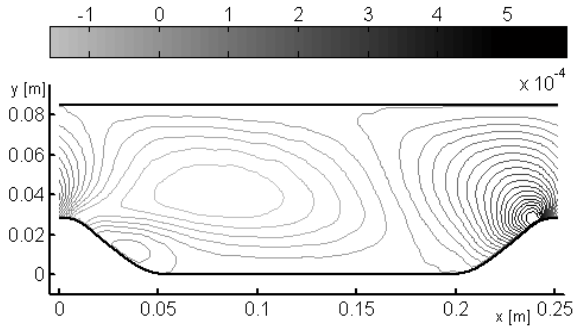

Fig. 4. Periodic hill flow: contours of velocity in y direction $[\mathrm{ms}^{-1}]$.

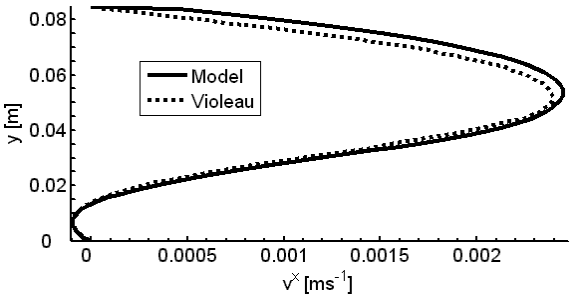

Fig. 5. Periodic hill flow: resulting velocity profile at $x = 0.056\,\mathrm{m}$ compared to data published in [11].

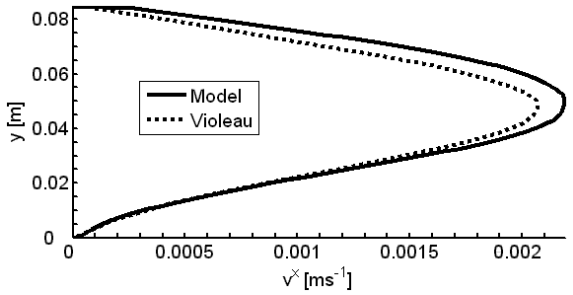

Fig. 6. Periodic hill flow: resulting velocity profile at $x = 0.14\,\mathrm{m}$ compared to data published in [11].

difference between resulting SPH flux and an appropriate analytic solution is less than 1% for all presenteded cases. In case, the rigid boundaries were represented by the boundary particles, the difference between computed fluxes and the analytic solution would grow up to 4%.

5.2. Periodic hill flow

The ability of the SPH code to capture the laminar flow along a curved boundary is tested on an example of a flow over a periodic hill, which narrows the horizontal channel by one third, [11]. The flow (which is evolved in time from the initial state when the fluid is at rest) is driven by a body force in longitudinal direction so that the resulting Reynolds number based on the hill height and the bulk velocity is 50. The length of the simulated channel section is nine times the hill height, which is $28\,\mathrm{mm}$. The modelled fluid is water. The periodic boundary conditions are applied in the direction of the flow. The rigid boundaries are modelled by the boundary particles. Representing the curved boundary by the ghost particles would become difficult as the reflection of particles and their velocities close to the convex as well as concave boundary curves is not trivial.

The contour plot of the resulting velocity distribution in x and y direction is shown on Fig. 3 and Fig. 4, respectively. As the SPH simulations are dynamic, slight numerical fluctuations in the resulting velocity distribution may be observed if the computation continues running after the steady state is reached. Due to this fact, Fig. 3 and Fig. 4 shows the averaged data which are obtained after the steady state. Despite the velocity fluctuations, the SPH solution remains stable while the numerical simulation keeps running. There is an obvious recirculation zone at the rear

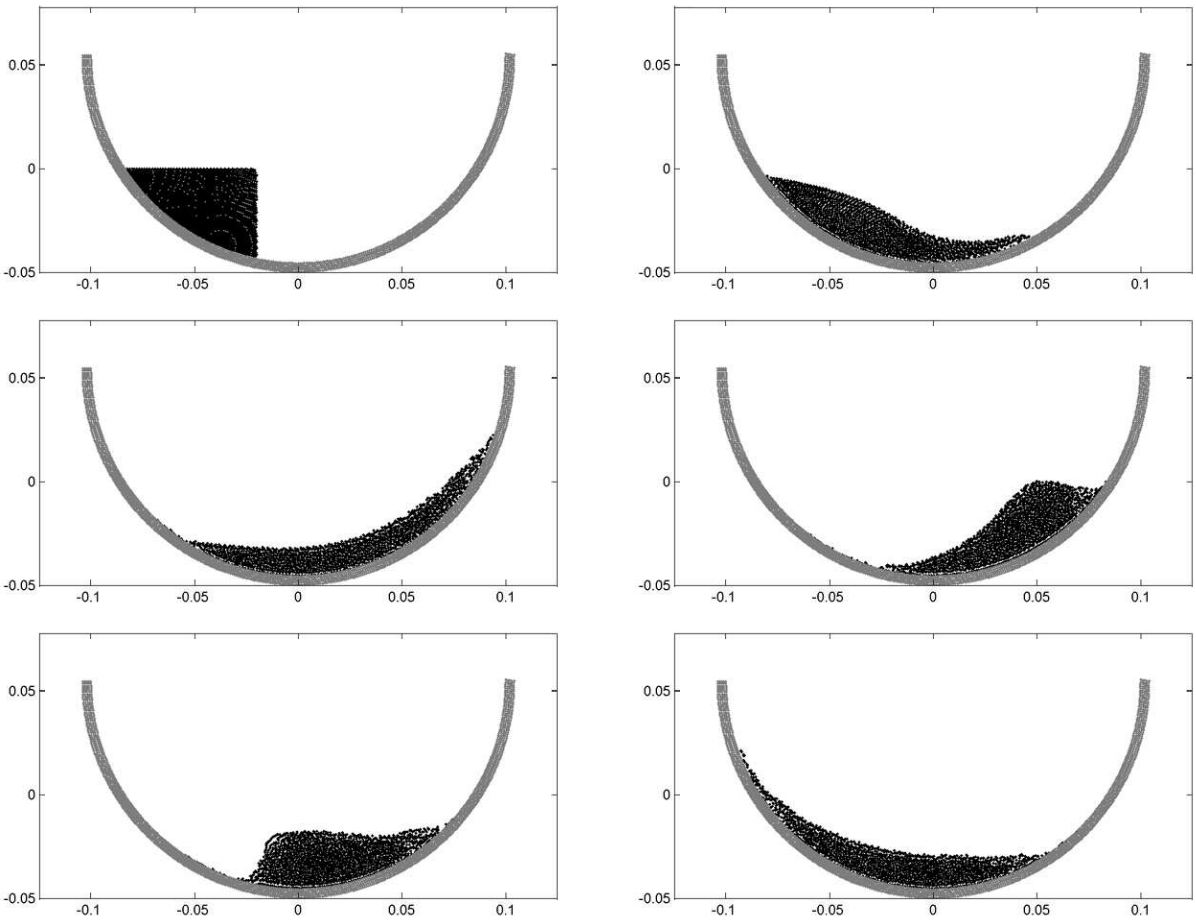

Fig. 7. Free surface flow in a cylindrical tube: fluid distribution at time $0.0\,\mathrm{s}$, $0.1\,\mathrm{s}$, $0.24\,\mathrm{s}$, $0.35\,\mathrm{s}$, $0.44\,\mathrm{s}$ and $0.55\,\mathrm{s}$.

part of the hill. That is apparent also on Fig. 5, where the resulting velocity profile through the channel cross-section at $x = 0.056\,\mathrm{m}$ is compared to the results published by Violeau and Issa in [11]. Fig. 6 compares the resulting profiles of the same authors at the position $x = 0.14\,\mathrm{m}$.

5.3. Free surface flow

The presented SPH incompressible fluid model is capable of simulating free surface flows without a need for a special treatment of the free surface boundary. This advantage of the SPH approach is often utilised within simulations of gravity current flows, e.g. [1], [7]. Within this study, the SPH ability to deal with a free surface boundary is presented on an example of a fluid which is settling down in a cylindrical tank after a sudden removal of a vertical dam, Fig. 7. This example also shows the applicability of the presented curved boundary implementation involving the boundary particles. The initial configuration of the simulation is apparent from the top left frame on Fig. 7. The cylinder radius is $x = 0.05\,\mathrm{m}$, the simulated fluid is water and the tank bottom is dry initially. The gravity force $x = 9.81\,\mathrm{ms}^{-2}$ acts in the vertical direction. After a dam removal, the fluid wave moves towards the right side of the tank where it is slowed down at the steep slope and the backward facing wave is formed consequently. The fluid flows from side to side till it settles down.

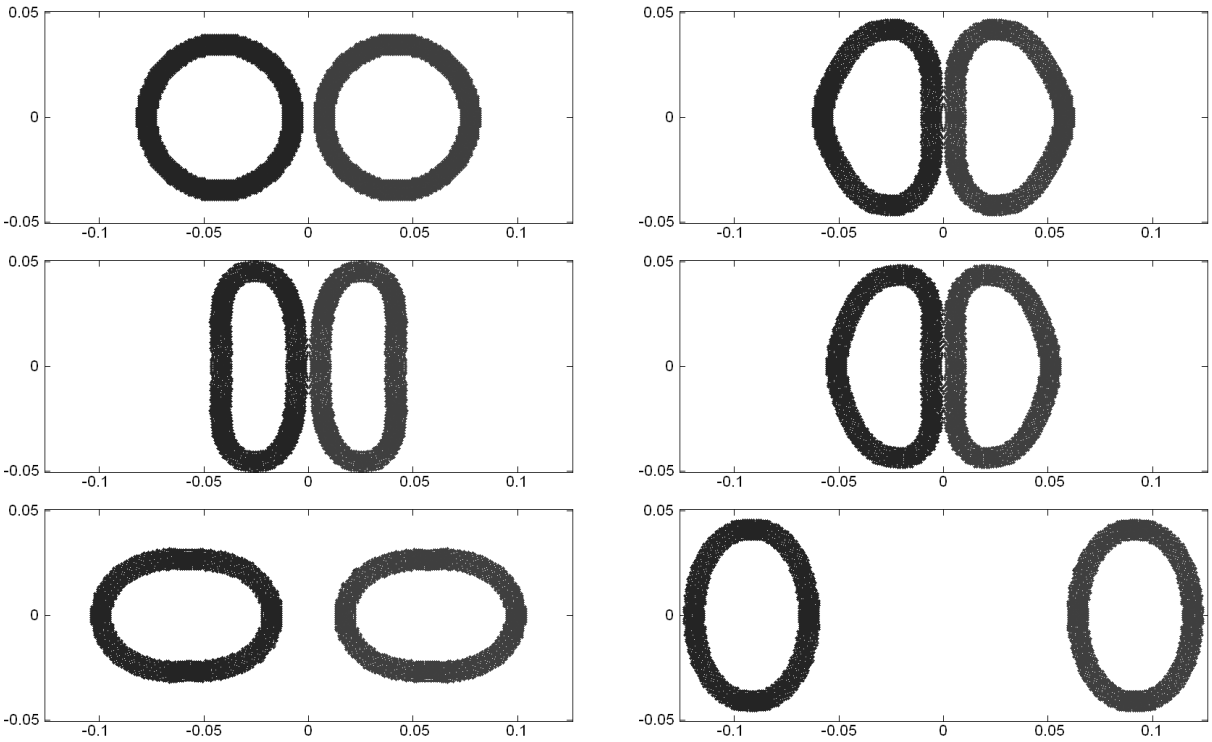

Fig. 8. Colliding rings: position at time $0.0\,\mathrm{s}$, $0.015\,\mathrm{s}$, $0.026\,\mathrm{s}$, $0.40\,\mathrm{s}$, $0.76\,\mathrm{s}$ and $1.10\,\mathrm{s}$.

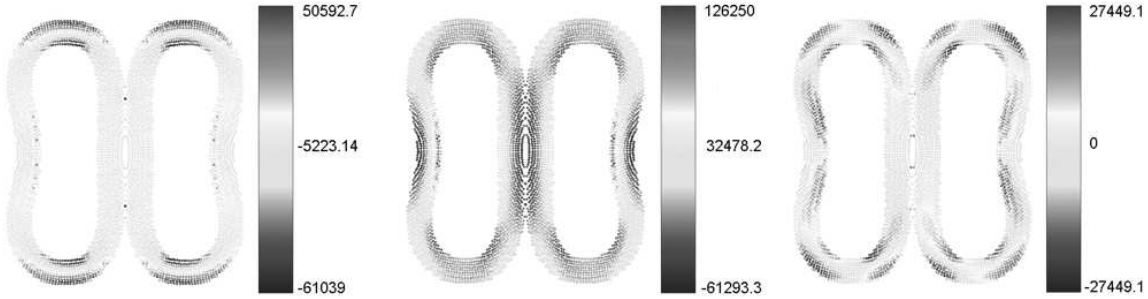

Fig. 9. Colliding rings: components of stress tensor σ_{xx}, σ_{yy} and σ_{xy} $[\mathrm{Pa}]$ at time $26\ \mathrm{ms}$.

5.4. Colliding rubber rings

The SPH model of elastic solid is applied to problem of colliding rubber rings, [3], where the rubber is modelled as an elastic material. The relative velocity of the rings at the moment of collision is equal to 0.12 times the soundspeed of the simulated material and the ratio between its shear modulus and its bulk modulus is 0.22 for the results presented on Fig. 8 and 0.11 for the results on Fig. 9. The ring thickness is equal to 0.25 times its outer diameter. The evolution of ring deformation in time is displayed on Fig. 8 and the contours of stress distribution in the deformed rings are visualised on Fig. 9. During the impact, rings become significantly deformed, afterthen they bounce off each other and travell appart while oscillating. During the simulation for the shear and bulk modulus ratio 0.22, the rings stay compact and keep oscillating till the simulation is stopped. The impact of the rings which ratio between shear and bulk modulus is equal to 0.11 results in numerical fragmentation. Fig. 9 presents the stress contours before the fragmentation occured. It is obvious that the absolute values of the stress components

are distributed symetrically across the impact plane. As expected, the highest values of the x component of the stress tensor are obtained in the region of the lower and the upper arch.

6. Conclusion

The SPH method is a numerical tool, which is able to analyse a wide range of physical processes. Its meshless character brings a number of advantages as well as disadvantages. It is capable of solving complex problems such as the free surface flow, but an SPH boundary definition may cause problems at some point. Eventhough a ghost particle boundary definition produces more accurate results for problems with a simple geometry, the boundary particles are feasible for the complex geometry simulations. The results of elastic material simulations are promising for the future work involving large deformations and the overall SPH character is promising for analysis of the fluid-structure interaction problems.

Acknowledgements

This work is supported by the research project MSM 4977751303 of the Ministry of Education, Youth and Sports of the Czech Republic.

References

[1] A. Colagrossi, M. Landrini, Numerical simulation of interfacial flows by smoothed particle hydrodynamics, Journal of Computational Physics 191 (2003) 448-475.

[2] R.A. Gingold, J.J. Monaghan, Smoothed Particle Hydrodynamics: theory and application to non-spherical stars, Monthly Notices of the Royal Astronomical Society 181 (1977) 375-389.

[3] J.P. Gray, J.J. Monaghan, R.P. Swift, SPH elastic dynamics, Computer Methods in Applied Mechanics and Engineering 190 (2001) 6641-6662.

[4] G.R. Liu, M.B. Liu, Smoothed Particle Hydrodynamics, World Scientific Publishing, Singapore, 2003.

[5] L. Lucy, A numerical approach to the testing of the fission hypothesis, Astronomical Journal 82 (1977) 1013-1020.

[6] J.J. Monaghan, Smoothed Particle Hydrodynamics, Annual Review of Astronomy and Astrophysics 30 (1992) 543-574.

[7] J.J. Monaghan, Simulating free surface flows with SPH, Journal of Computational Physics 110 (1994) 399-406.

[8] J.J. Monaghan, SPH without a tensile instability, Journal of Computational Physics 159 (2000) 290-311.

[9] J.J. Monaghan, R.A. Gingold, Shock simulation by the particle method SPH, Journal of Computational Physics 52 (1983) 374-389.

[10] J.P. Morris, P.J. Fox, Y. Zhu, Modeling low Reynolds number incompressible flows using SPH, Journal of Computational Physics 136 (1997) 214-226.

[11] D. Violeau, R. Issa, Numerical modelling of complex turbulent free-surface flows with the SPH method: an overview, International Journal for Numerical Methods in Fluids 53 (2007) 277-304.